Predictive Modeling of External Noise Emissions from Transverse Rumble Strips Using Acoustic Simulation Techniques

Ahmad Fajar[1] **and Rizky Aditya Putra**[2]
[1] Department of Civil Engineering, Universitas Luhur Paramarta,, Jalan Diponegoro–Purwokerto Utara, Purwokerto, Indonesia
[2]Department of Computer Science and Engineering, Universitas Samudra,, 89 Jalan Meurandeh–Langsa Timur, Langsa 24416, Indonesia

ABSTRACT Road traffic noise is a persistent environmental exposure for communities near highways and arterials, and it is shaped not only by vehicle flow and speed but also by roadway surface features intended for safety. Transverse rumble strips introduce deliberate geometric discontinuities that improve driver alertness, yet the same discontinuities can elevate exterior acoustic emissions through impulsive tire–pavement excitation. This paper develops a predictive modeling framework for external noise from transverse rumble strips that integrates mechanistic source characterization with acoustic simulation and data-driven regression. The approach treats rumble-strip geometry and operating conditions as parametric inputs, converts tire–strip interaction into an equivalent distributed boundary excitation, and propagates the resulting sound field through a computational domain that captures near-field scattering and far-field radiation. Frequency-resolved emission descriptors are computed from simulated pressure time histories to support both regulatory-style metrics and diagnostic spectral signatures. Statistical learning is then used to map design and operating variables to sound pressure level outcomes while quantifying uncertainty and separating systematic effects from stochastic variability. The resulting workflow supports rapid evaluation of alternative rumble-strip geometries under constraints on safety-relevant vibration and provides a technical basis for balancing alerting effectiveness against external noise impacts without relying solely on extensive field campaigns.

1. Introduction

Transverse rumble strips are intentionally patterned features placed across the travel path so that a vehicle traversing them experiences oscillatory excitation, generating tactile and audible feedback for the driver [1]. Their safety purpose is to increase driver awareness, particularly where lane departure or approach-speed management is a concern. From an exterior-noise perspective, however, the same mechanism that produces driver-perceptible cues can increase sound radiated by the tire, the vehicle underbody, and the adjacent roadway structure. The resulting acoustic field is not a simple broadband increase; it often contains strong tonal or quasi-tonal components tied to strip spacing and vehicle speed, transient components tied to entry and exit events, and amplitude modulation linked to axle spacing, suspension dynamics, and tire tread pattern. Predicting exterior emissions is therefore a multi-physics problem in which contact mechanics, structural vibration, and acoustic radiation interact across multiple time and length scales.

Field measurements remain essential for characterizing real-world impacts, but they face practical constraints. Ambient wind, temperature gradients, nearby reflecting surfaces, traffic heterogeneity, and microphone placement variability can obscure causal links between rumble-strip geometry and measured sound levels. Moreover, measurements provide limited information about counterfactual designs that are not yet built. A predictive framework that combines acoustic simulation with data-driven inference can address these limitations by

Article info:
Ahmad Fajar and Rizky Aditya Putra. *Predictive Modeling of External Noise Emissions from Transverse Rumble Strips Using Acoustic Simulation Techniques*. Center for Theoretical and Applied STEM Research (CTASR) . Licensed under Attribution - NonCommercial - No Derivatives 4.0 International (CC BY-NC-ND 4.0)

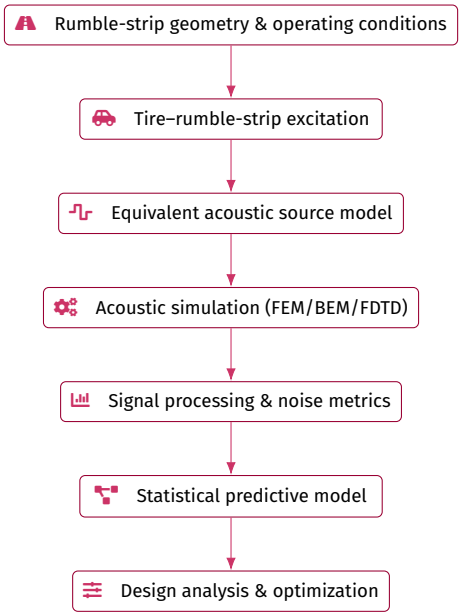


Figure 1 Overall modeling workflow for predicting exterior noise from transverse rumble strips. Parametric rumble-strip geometry and operating conditions drive a mechanistic tire–strip excitation model, which is converted to an equivalent acoustic source representation compatible with numerical propagation solvers. Frequency- and time-domain simulations yield receiver pressure histories that are post-processed into decibel and spectral metrics, and these outputs feed a statistical learner that delivers uncertainty-aware predictions and supports optimization of rumble-strip designs under safety and noise constraints.

enabling systematic parametric sweeps, controlled isolation of variables, and uncertainty quantification. Such a framework is also useful when the design objective is not merely to predict noise, but to understand how design modifications redistribute acoustic energy across frequency bands that align with human perception, building façade transmission, or regulatory weighting curves.

The modeling challenge begins at the source [2]. A tire rolling over transverse grooves or bars experiences a sequence of vertical displacements and force perturbations at the contact patch. These perturbations depend on groove depth and width, edge sharpness, spacing, and the compliance of both the tire and the pavement. The tire response includes rigid-body and flexible modes, with the latter contributing to radiation efficiency as the vibrating sidewall and tread act as distributed acoustic sources. Additionally, the underbody cavity and wheel well can act as resonant scatterers that shape the emitted spectrum. For exterior receivers, propagation further filters the source through geometric spreading, ground interference, atmospheric absorption, and scattering by roadside terrain or barriers. A credible prediction model must therefore represent source excitation, radiation, and propagation in a way that is parameterized, computationally tractable, and compatible with statistical learning.

Acoustic simulation techniques provide a structured path forward. In the frequency domain, the linearized acoustic field in homogeneous media can be represented by the Helmholtz equation, and radiating solutions can be obtained using finite element methods (FEM) in bounded domains coupled to radiation conditions, or boundary element methods (BEM) in unbounded domains. In the time domain, finite-difference time-domain (FDTD) or discontinuous Galerkin methods can capture transient impulses and nonstationary modulation, at the cost of more stringent stability and resolution requirements. Because rumble-strip noise includes both transient and periodic features, a hybrid workflow is attractive: generate a physically interpretable excitation model, compute acoustic transfer functions using frequency-domain solvers, and reconstruct time histories via convolution or inverse transforms, while also allowing direct transient simulation when needed for entry and exit events [3].

Yet simulation alone is rarely sufficient for practical design decisions. Even when geometry is precisely known, uncertainty in tire properties, vehicle fleet composition, and operational conditions can dominate prediction error. A statistical layer is therefore needed to connect simulation outputs with observed variability and to provide predictive distributions rather than single deterministic values. This motivates a two-level model: a mechanistic simulation generates physically constrained features, and a statistical learner maps those features and input parameters to predicted external noise metrics while estimating uncertainty and enabling hypothesis tests about design effects. Such an approach can also support calibration, where a limited set of measurements is used to tune uncertain parameters in the simulation so that extrapolation to new designs is less speculative.

This paper presents an integrated framework for

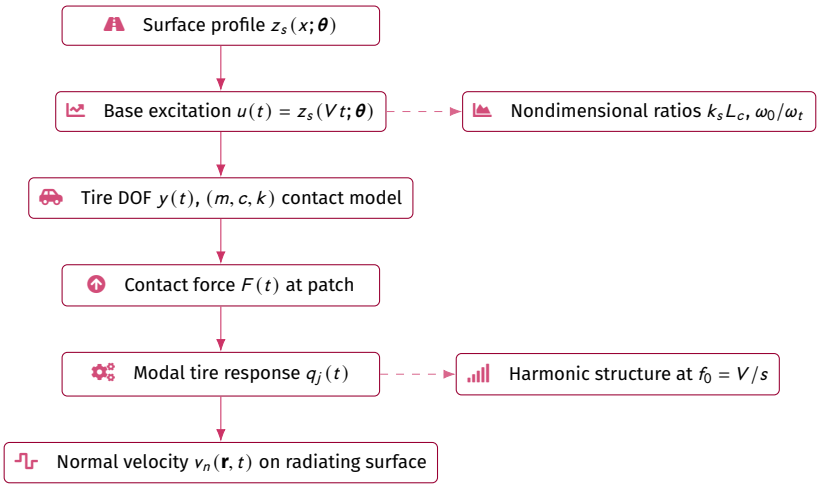


Figure 2 Mechanistic source characterization mapping rumble-strip geometry to acoustic boundary excitation. The transverse profile and spacing define a base excitation that is filtered through an effective tire contact model to produce a contact force sequence, which in turn excites reduced-order tire modes and yields an equivalent normal velocity distribution on radiating surfaces. Nondimensional parameters such as the strip wavenumber relative to contact-patch length and the ratio of encounter frequency to tire resonances organize the response, while the resulting harmonic structure and modal content provide physically interpretable features for downstream acoustic radiation and statistical learning.

predictive modeling of external noise emissions from transverse rumble strips using acoustic simulation techniques. The development proceeds by formalizing the tire–rumble-strip interaction as a parametric excitation process and by defining equivalent acoustic source representations suitable for numerical propagation models. It then details numerical discretization strategies for near-field and far-field acoustics, including coupled FEM–BEM formulations and absorbing boundary treatments, together with resolution criteria tied to frequency content and strip spacing. Next, it defines frequency-spectrum and decibel-based descriptors that translate simulated pressure signals into metrics used for comparison and design, including weighted levels, band-limited levels, and time–frequency energy maps. Finally, it constructs statistical predictive models that combine simulated features with parametric inputs, applying regression, regularization, Gaussian-process-style correlation structures, and hypothesis testing to quantify the influence of design parameters and to produce uncertainty-aware predictions. The framework is oriented toward engineering use where the goal is not only to forecast noise levels, but to provide interpretable sensitivities and optimization pathways for geometry modification under operational constraints.

2. Mechanistic Source Characterization of Tire–Rumble-Strip Excitation

A transverse rumble strip can be idealized as a repeating geometric profile along the travel direction, with a characteristic spacing that converts vehicle speed into an excitation frequency. Let the longitudinal coordinate along the lane centerline be denoted by x, and let the rumble-strip surface elevation relative to a nominal road plane be $z_s(x;\boldsymbol{\theta})$, where $\boldsymbol{\theta}$ encodes geometric parameters such as groove depth, groove width, edge radius, strip spacing, and pattern length. For a vehicle traveling at speed V, the contact patch experiences the surface profile as a time signal $z_s(Vt;\boldsymbol{\theta})$ in the simplest kinematic mapping. This mapping is only a starting point because the tire filters the imposed displacement through compliance, damping, and internal structural dynamics, and because the contact mechanics mediate whether the tread follows the groove bottom or bridges across it.

A common modeling approach is to represent the vertical interaction at the contact patch through an equivalent linear time-invariant system in which the pavement profile acts as a base excitation. Let $y(t)$ denote an effective vertical degree of freedom representing the tire belt or unsprung mass displacement at the patch, and let the road input be $u(t) = z_s(Vt;\boldsymbol{\theta})$. A minimal linear model is

$$m\ddot{y}(t) + c\dot{y}(t) + ky(t) = ku(t) + c\dot{u}(t),$$

where m is an effective mass, c an effective damping, and k an effective stiffness. The contact force transmitted to the pavement or radiating structure can be approximated as

$$F(t) = k\big(y(t) - u(t)\big) + c\big(\dot{y}(t) - \dot{u}(t)\big).$$

While this representation is simplified, it highlights two key facts: the excitation is shaped by both the geometry $u(t)$ and the dynamical filter defined by (m, c, k), and the force contains contributions proportional to relative displacement and velocity, thereby amplifying sharp edges and high-frequency components of the strip profile. More elaborate models embed multiple modes for the tire belt and sidewall, incorporate nonlinear stiffness or contact

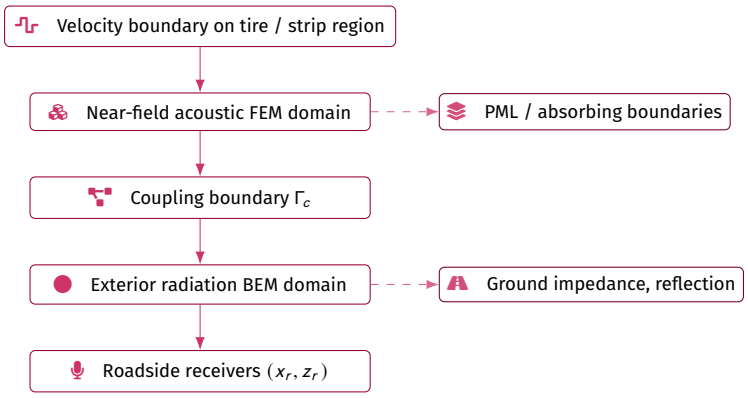


Figure 3 Numerical acoustic domain decomposition used to propagate rumble-strip excitation to roadside receivers. Equivalent velocity boundary conditions derived from the tire–strip interaction drive a near-field acoustic finite-element model, which is truncated with absorbing layers and coupled across an interface to a boundary-element representation of the unbounded exterior field. Ground reflection and impedance effects are incorporated through boundary conditions in the exterior domain, enabling prediction of level and spectral variations with receiver position while keeping the spatial discretization concentrated near the geometrically complex source region.

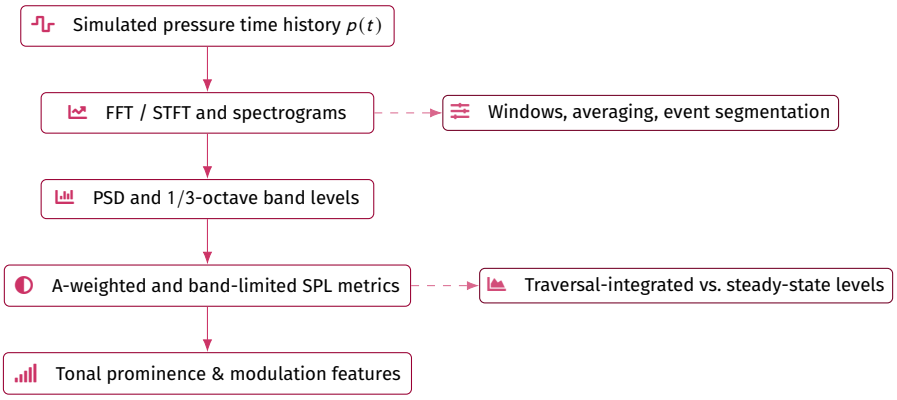


Figure 4 Signal-processing chain converting simulated acoustic pressures into noise descriptors suitable for design and assessment. Time-domain pressure histories from the acoustic solver are transformed into frequency and time–frequency representations, from which power spectral densities and band levels are derived. Weighting operations, windowing choices, and traversal segmentation distinguish steady-periodic contributions from transient entry and exit events, while additional descriptors such as tonal prominence and modulation features capture features of rumble-strip noise that are not reflected in overall A-weighted sound-pressure levels alone.

loss, or represent the contact patch as a distributed region rather than a point. In practice, the modeling choice can be aligned with the intended frequency range and with the computational budget of the coupled acoustic simulation.

The periodicity of transverse rumble strips implies that a large portion of the excitation is quasi-periodic when the vehicle remains centered and maintains approximately constant speed [4]. If the strip spacing is s, then the nominal encounter rate is $f_0 = V/s$. The excitation spectrum contains a fundamental near f_0 and harmonics due to non-sinusoidal profile shapes and edge discontinuities. For a profile $z_s(x)$ that is periodic with period s, the Fourier series representation can be written as

$$z_s(x) = \sum_{n=-\infty}^{\infty} Z_n e^{i2\pi nx/s},$$

which, under the mapping $x = Vt$, yields temporal frequencies $f_n = nV/s$. The force spectrum is then shaped by the mechanical transfer function of the tire–suspension system. In the frequency domain, if $Y(\omega)$ and $U(\omega)$ are the Fourier transforms of $y(t)$ and $u(t)$, the transfer from base input to relative displacement is

$$\frac{Y(\omega) - U(\omega)}{U(\omega)} = -\frac{m\omega^2}{k - m\omega^2 + ic\omega},$$

which emphasizes frequencies near resonance where $k \approx m\omega^2$ and attenuates very low frequencies where the tire follows the base motion. This suggests that rumble-strip spacing that aligns f_0 or low-order harmonics with dominant tire or suspension resonances can increase radiated noise, even if the geometric amplitude is unchanged.

The excitation also couples to structural vibration of

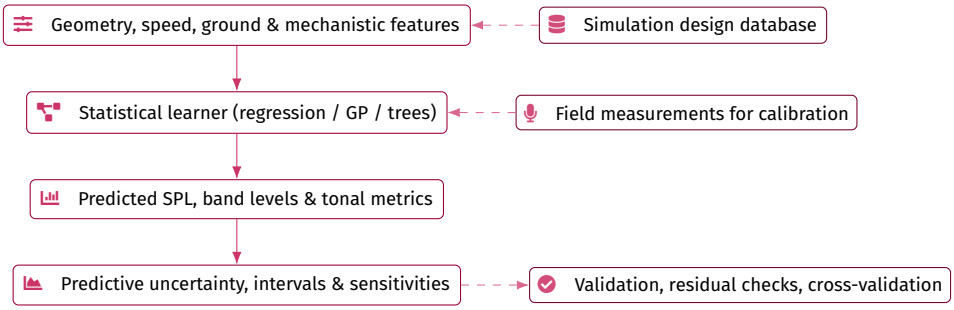


Figure 5 Data-driven prediction layer that compresses simulation and measurement information into fast surrogate models. Parametric descriptors of geometry, operating conditions, and mechanistic outputs populate a design database that trains a flexible learner to map inputs to external noise metrics. Field measurements provide calibration and model-discrepancy information, while predictive uncertainty and sensitivity measures are used to quantify confidence, support hypothesis tests about geometric effects, and identify directions in parameter space that most strongly influence external rumble-strip noise.

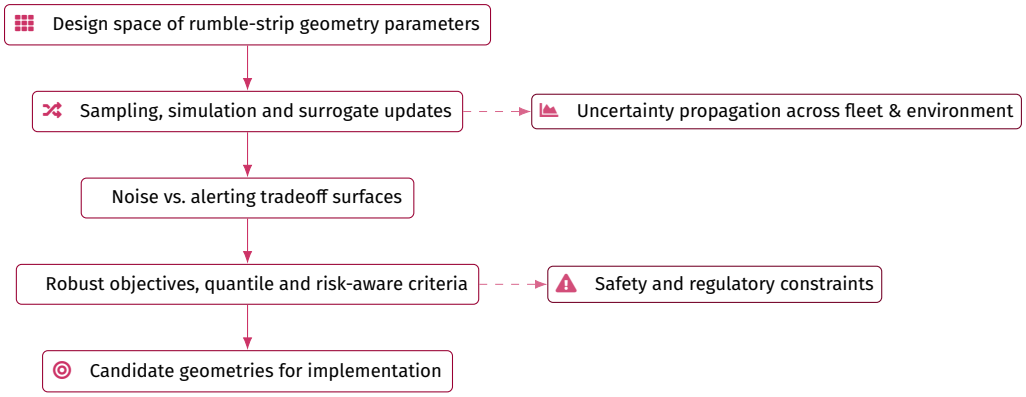


Figure 6 Parametric analysis and optimization layer for balancing exterior noise with safety-related performance. The framework explores a design space of rumble-strip geometry through sampled simulations and surrogate models, building tradeoff surfaces that relate external acoustic metrics to alerting proxies. Uncertainty propagation over vehicle fleets and environmental conditions informs robust and quantile-based objectives, while explicit constraints enforce minimum safety performance and compatibility with noise regulations, leading to candidate geometries that reflect both physical variability and modeling limitations.

the pavement and adjacent components. The pavement can be idealized, over a limited region, as an elastic plate on a foundation, with the rumble strip acting as a localized stiffness and mass perturbation [5]. Let $w(\mathbf{r}, t)$ denote vertical deflection of the pavement surface at planar coordinate $\mathbf{r} = (x, y)$, and consider a plate equation of the form

$$D\nabla^4 w(\mathbf{r}, t) + \rho_p h \ddot{w}(\mathbf{r}, t) + \eta \dot{w}(\mathbf{r}, t) + K_f w(\mathbf{r}, t) = p_c(\mathbf{r}, t),$$

where D is bending stiffness, ρ_p density, h thickness, η damping, K_f a foundation stiffness, and p_c the contact pressure distribution. Although exterior airborne noise is often dominated by the tire itself, pavement vibration can contribute, especially when grooves induce higher contact-force variation or when the pavement includes features that increase radiation efficiency. Even when the pavement contribution is small, pavement compliance influences the contact force and thus the tire vibration, making it relevant indirectly.

To translate the mechanical excitation into an acoustic source model, a useful abstraction is an equivalent normal velocity boundary condition on a radiating surface. Suppose a portion of the tire sidewall or tread surface is represented by a boundary Γ with outward normal $\mathbf{n}$. If the local normal velocity is $v_n(\mathbf{r}, t)$, then in linear acoustics the radiated field can be computed from boundary integral or FEM formulations. The challenge is to obtain v_n from the mechanical excitation model without simulating the full tire structure. One route is to use an empirical or reduced-order radiation model in which the contact force $F(t)$ excites a small set of vibration modes whose shapes $\phi_j(\mathbf{r})$ and modal coordinates $q_j(t)$ satisfy

$$\ddot{q}_j(t) + 2\zeta_j \omega_j \dot{q}_j(t) + \omega_j^2 q_j(t) = \alpha_j F(t),$$

with ω_j modal frequencies, ζ_j damping ratios, and α_j participation factors. The normal velocity is then approximated as

$$v_n(\mathbf{r}, t) \approx \sum_{j=1}^{J} \dot{q}_j(t) \phi_j(\mathbf{r}).$$

This representation is attractive because it can be parameterized and calibrated, and it naturally produces

resonant peaks in the radiated spectrum. It also enables separation between a quasi-periodic component driven by the strip sequence and a stochastic component driven by tread pattern, lateral wander, and microtexture.

Because the excitation is speed dependent, it is convenient to define nondimensional parameters that organize the response [6]. A key ratio compares the excitation wavelength in space to the contact patch length L_c. The spatial wavenumber of the strip pattern is $k_s = 2\pi/s$, and a nondimensional measure is $k_s L_c$. When $k_s L_c \ll 1$, the contact patch averages the profile, reducing force variation; when $k_s L_c \gtrsim 1$, the patch resolves the periodic features, increasing force modulation. A second ratio compares the excitation frequency to a representative tire resonance, ω_0/ω_t, where $\omega_0 = 2\pi V/s$. These ratios can be used as features in predictive models and can guide mesh and timestep requirements in numerical simulations.

In external noise prediction, it is often necessary to distinguish between near-field emissions close to the wheel and far-field levels at roadside receptors. The source model must therefore be compatible with radiation calculations over a range of distances. An effective strategy is to compute a source strength in terms of equivalent volume velocity $Q(t)$ or surface velocity distribution $v_n(\mathbf{r}, t)$ and to couple it to propagation models that include ground and atmospheric effects. For example, if the source is approximated as a compact monopole for low frequencies, the radiated pressure at distance R in free field is

$$p(t) \approx \frac{\rho_0}{4\pi R} \frac{dQ(t - R/c_0)}{dt},$$

with ambient density ρ_0 and sound speed c_0. For higher frequencies where the source is not compact, directivity and interference effects become important, motivating the use of distributed boundary sources in numerical solvers [7]. The remainder of the framework therefore focuses on simulation methods capable of handling both compact and distributed radiation in a parameterized setting.

3. Acoustic Simulation Techniques and Numerical Discretization

The acoustic field generated by rumble-strip excitation is typically well described by linear acoustics in air for the sound-pressure levels and distances relevant to environmental assessment, provided that nonlinear propagation effects are negligible. Under the assumption of time-harmonic dependence $e^{i\omega t}$, the acoustic pressure $p(\mathbf{x}, \omega)$ in a homogeneous medium satisfies the Helmholtz equation

$$\nabla^2 p(\mathbf{x}, \omega) + k^2 p(\mathbf{x}, \omega) = 0,$$

where $k = \omega/c_0$ is the acoustic wavenumber. Boundary conditions encode the coupling to vibrating surfaces and impedance effects. On a vibrating boundary Γ_v with prescribed normal velocity $v_n(\mathbf{x}, \omega)$, a Neumann condition is

$$\frac{\partial p}{\partial n}(\mathbf{x}, \omega) = -i\omega\rho_0 v_n(\mathbf{x}, \omega), \quad \mathbf{x} \in \Gamma_v.$$

On an impedance boundary Γ_z that models energy absorption or porosity, an admittance condition can be written as

$$\frac{\partial p}{\partial n} = -ik\beta(\omega)p,$$

where $\beta(\omega)$ relates to normalized surface impedance. These expressions provide a direct interface between the source characterization described previously and the propagation solver.

Finite element methods discretize the Helmholtz equation in a bounded domain Ω containing the source and near-field region. The weak form is obtained by multiplying by a test function w and integrating by parts:

$$\int_\Omega \nabla w \cdot \nabla p \, d\Omega - k^2 \int_\Omega w p \, d\Omega - \int_{\partial\Omega} w \frac{\partial p}{\partial n} \, d\Gamma = 0.$$

Boundary integrals incorporate Neumann excitation and radiation conditions. Because the physical domain is unbounded, truncation is required, and the outer boundary must approximate outgoing waves [8]. One approach is to use absorbing boundary conditions such as a first-order Sommerfeld condition,

$$\frac{\partial p}{\partial n} = ikp,$$

on an artificial boundary sufficiently far from the source. A more robust approach uses perfectly matched layers (PML), which introduce complex coordinate stretching to attenuate outgoing waves without reflection. In practice, PML implementation requires careful selection of layer thickness and attenuation profile to avoid numerical reflection at discrete interfaces.

Discretization leads to a complex-valued linear system

$$\mathbf{K}\mathbf{p} = \mathbf{f},$$

where $\mathbf{K}$ includes stiffness-like and mass-like terms and boundary contributions, and $\mathbf{f}$ encodes Neumann excitation from vibrating surfaces. The system is indefinite for many frequencies, and solver choice matters. Direct factorization is robust for moderate sizes but expensive for high-frequency 3D problems; iterative Krylov methods with suitable preconditioning are often required. Because rumble-strip noise can include significant energy up to several kilohertz depending on speed and geometry, the mesh resolution must satisfy wavelength criteria. A common guideline is to use at least N_λ nodes per wavelength, often with N_λ between 6 and 12 depending on element order and desired accuracy. If the maximum frequency of interest is $f_{\max}$, then the smallest wavelength is $\lambda_{\min} = c_0/f_{\max}$, and the characteristic element size h_e should satisfy $h_e \lesssim \lambda_{\min}/N_\lambda$. This requirement can make

Layer	Primary role	Representative methods / outputs
Mechanistic source characterization	Map rumble-strip geometry and speed to contact excitation	Parametric surface profile $z_s(x;\boldsymbol{\theta})$, base-excited tire model, modal radiation surrogates
Acoustic propagation	Compute near- and far-field sound radiation	Helmholtz FEM, BEM, FEM–BEM coupling, time-domain wave solvers, transfer functions
Signal processing	Transform pressure time histories into noise metrics	SPL, A-weighted levels, band levels, PSDs, spectrograms, tonal indicators
Statistical prediction	Relate inputs and simulated features to noise metrics with uncertainty	Regression, Gaussian-process emulators, regularization, multi-output models
Parametric analysis and optimization	Explore design space and tradeoffs under uncertainty	Sensitivity maps, robust objectives, multi-fidelity optimization, constraint handling

Table 1 Key components of the integrated framework for predicting external noise from transverse rumble strips.

full-domain FEM expensive, motivating hybrid methods [9].

Boundary element methods are attractive for exterior acoustics because they satisfy the radiation condition inherently by using Green's functions in an unbounded domain. For the Helmholtz equation, the free-space Green's function is

$$G(\mathbf{x},\mathbf{y}) = \frac{e^{ik|\mathbf{x}-\mathbf{y}|}}{4\pi|\mathbf{x}-\mathbf{y}|}.$$

Using boundary integral identities, the pressure at a field point can be expressed in terms of boundary pressure and its normal derivative. A representative boundary integral equation on a boundary Γ is

$$\frac{1}{2}p(\mathbf{x}) = \int_\Gamma \left(G(\mathbf{x},\mathbf{y})\frac{\partial p}{\partial n}(\mathbf{y}) - p(\mathbf{y})\frac{\partial G}{\partial n_y}(\mathbf{x},\mathbf{y}) \right) d\Gamma(\mathbf{y}), \quad \mathbf{x}\in\Gamma.$$

With Neumann data from a prescribed normal velocity, one can solve for boundary pressure and then evaluate the field at receiver points. BEM reduces the dimensionality of the mesh by one, but it yields dense matrices and can suffer from irregular-frequency issues unless stabilized. Fast multipole acceleration or hierarchical matrix compression can reduce computational complexity, enabling parametric sweeps needed for predictive modeling.

A practical strategy for rumble-strip noise is FEM–BEM coupling. FEM is used to represent the complex near-field region that includes the tire, wheel well, and possibly ground impedance variations, while BEM provides an efficient radiation representation for the unbounded exterior. Coupling can be accomplished by enforcing continuity of pressure and normal velocity on an interface boundary Γ_c that encloses the near-field region [10]. In one formulation, FEM solves the interior problem with unknown boundary pressure on Γ_c, while BEM provides a Dirichlet-to-Neumann map that relates pressure on Γ_c to its normal derivative consistent with outgoing waves. The coupled system can be written abstractly as

$$\begin{bmatrix} \mathbf{K}_{\text{FEM}} & \mathbf{C} \\ \mathbf{C}^\top & \mathbf{K}_{\text{BEM}} \end{bmatrix} \begin{bmatrix} \mathbf{p}_{\text{int}} \\ \mathbf{p}_{\Gamma_c} \end{bmatrix} = \begin{bmatrix} \mathbf{f}_{\text{int}} \\ 0 \end{bmatrix},$$

where $\mathbf{p}_{\Gamma_c}$ denotes degrees of freedom on the coupling boundary. The principal value of this approach is that the computationally demanding discretization is concentrated where geometric complexity is high, while the far field is handled analytically through boundary integrals.

Time-domain simulation is useful when the excitation is strongly transient, such as the first and last strip impacts, or when one wants to model nonstationary speed or lateral wander. In a simple second-order wave equation form,

$$\frac{1}{c_0^2}\frac{\partial^2 p}{\partial t^2} - \nabla^2 p = s(\mathbf{x},t),$$

a finite-difference time-domain method discretizes both space and time. Stability is governed by a Courant condition; for a uniform grid spacing Δx in 3D, a typical requirement is

$$\Delta t \le \frac{\Delta x}{c_0\sqrt{3}}.$$

This can be restrictive at high frequencies. Nevertheless, a time-domain solver can be combined with model-order reduction or with band-limited excitation to focus on the most relevant frequencies. Another time-domain route is to use impulse-response modeling: compute frequency-domain transfer functions from source surfaces to receiver points and then apply inverse transforms to obtain time signals for arbitrary force inputs [11]. If $H(\omega)$ is the transfer function from a source volume velocity $Q(\omega)$ to

Symbol	Quantity	Role in modeling tire–strip excitation
s	Strip spacing	Sets encounter frequency $f_0 = V/s$ and harmonic structure of excitation
d_g	Groove depth	Controls vertical displacement amplitude and low-frequency force variation
w_g	Groove width	Influences contact patch bridging and effective sharpness of profile edges
r_e	Edge radius	Governs high-frequency content via impulsiveness of tire entry and exit
L_p	Pattern length	Determines number of effective encounters per traversal and build-up to steady state
V	Vehicle speed	Scales temporal mapping $x = Vt$ and shifts harmonic frequencies across bands
L_c	Contact patch length	Enters nondimensional ratio $k_s L_c$ that controls geometric averaging of the profile

Table 2 Geometric and operational parameters that define the rumble-strip excitation environment.

pressure at a receiver, then

$$P(\omega) = H(\omega)Q(\omega),$$

and the time signal is obtained by inverse Fourier transform with suitable windowing to control wrap-around effects.

Numerical simulation of rumble-strip noise also requires representing the ground. The ground can be modeled as a rigid plane, an impedance boundary, or a layered medium. A rigid plane yields strong interference patterns due to mirror-image sources, often producing pronounced spectral ripples at receivers. An impedance boundary smooths this interference by dissipating energy and altering the reflection phase. In frequency-domain models, a locally reacting impedance condition can be used, but it may not fully capture grazing-incidence behavior over porous grounds. A compromise is to use an effective impedance model that is calibrated against typical ground types, treated as uncertain in the statistical layer. For road-adjacent receivers, the height above ground and the source height at the wheel are critical, because small changes can shift interference minima and maxima across bands, affecting A-weighted levels even when unweighted energy is similar.

The final element of simulation concerns computational efficiency for parametric studies [12]. Rumble-strip prediction often requires exploring a design space of groove depth, spacing, pattern length, and edge shape, as well as operational variables such as speed and lateral offset. Direct high-fidelity simulation for every design point can be prohibitive. Two efficiency approaches are therefore integrated: precompute acoustic transfer functions for a fixed geometry and vary only excitation, and build surrogate models that approximate simulation outputs as smooth functions of input parameters. In the first approach, the geometry-dependent transfer matrix from boundary velocity degrees of freedom to receiver pressure is computed once per geometry, enabling rapid evaluation across speeds and excitation realizations. In the surrogate approach, a limited set of simulations is used to train an emulator such as a Gaussian-process regression or polynomial chaos expansion, reducing the number of expensive solves required for optimization and uncertainty propagation.

4. Frequency Spectrum Analysis, Decibel Metrics, and Propagation Modeling

External noise assessment relies on signal processing that converts simulated or measured pressure time histo-

Quantity	Definition	Physical interpretation	Domain
$u(t)$	$z_s(Vt;\boldsymbol{\theta})$	Effective base displacement imposed by strip profile at the contact patch	Source
$y(t)$	Tire / unsprung mass vertical DOF	Filtered response of tire–suspension system to $u(t)$	Structural
$F(t)$	$k(y-u)+c(\dot{y}-\dot{u})$	Contact force driving tire vibration and pavement loading	Coupling
f_0	V/s	Fundamental encounter frequency associated with strip spacing	Spectral
$k_s L_c$	$(2\pi/s)L_c$	Measure of whether the contact patch averages or resolves strip geometry	Nondimensional
ω_0/ω_t	$(2\pi V/s)/\omega_t$	Ratio of excitation to tire resonance, indicating potential amplification	Scaling

Table 3 Representative dynamical quantities governing tire–rumble-strip interaction and resulting excitation spectra.

Acoustic approach	Strengths for rumble-strip problems	Typical limitations / preferred use
Frequency-domain FEM	Handles complex near-field geometry and impedance boundaries	Requires domain truncation and fine meshes at high frequencies; best for moderate 3D bands
Boundary element method (BEM)	Naturally enforces radiation in unbounded exterior domains	Dense matrices, irregular-frequency issues; efficient with fast multipole or for few frequencies
Coupled FEM–BEM	Concentrates discretization near source while treating far field analytically	More complex implementation; attractive for detailed wheel-well and ground modeling
Time-domain wave / FDTD	Captures transients, entry/exit events, and modulation effects	Courant timestep constraints and long run times at kilohertz frequencies; useful for selected scenarios

Table 4 Comparison of acoustic simulation strategies for modeling radiation from rumble-strip-induced excitation.

ries into standardized descriptors. For a pressure signal $p(t)$ at a receiver, the root-mean-square pressure over a window of duration T is

$$p_{\mathrm{rms}} = \sqrt{\frac{1}{T}\int_{t_0}^{t_0+T} p^2(t)\,dt}.$$

Sound pressure level (SPL) in decibels is then defined as

$$L_p = 20\log_{10}\left(\frac{p_{\mathrm{rms}}}{p_{\mathrm{ref}}}\right),$$

where p_{ref} is a reference pressure, commonly $20\,\mu$Pa in air. Because rumble-strip noise is often nonstationary, the choice of windowing affects p_{rms} and therefore L_p. For a vehicle traversing a finite strip array, it is useful to compute both a traversal-integrated metric, which captures total exposure over the event, and a steady-state metric computed over the central portion where periodicity is established. This distinction can be represented by selecting different T and window locations [13].

Frequency-domain descriptors are essential because rumble-strip excitation can concentrate energy at harmonics of the encounter rate. The discrete Fourier transform of a sampled signal $p[n] = p(n\Delta t)$ for $n = 0,\ldots,N-1$ is

$$P[k] = \sum_{n=0}^{N-1} p[n]e^{-i2\pi kn/N},$$

with frequency bins $f_k = k/(N\Delta t)$. The power spectral density (PSD) can be estimated as

$$S_{pp}(f_k) = \frac{2\Delta t}{N}|P[k]|^2,$$

for one-sided spectra under appropriate conventions.

Target quantity	Symbol / relation	Guideline	Implication for simulations
Maximum frequency of interest	$f_{\max}$	Chosen from expected harmonic content and regulatory bands	Sets smallest wavelength and strongest mesh constraints
Smallest wavelength	$\lambda_{\min} = c_0/f_{\max}$	Derived from $f_{\max}$ and sound speed c_0	Basis for element-size and timestep criteria
Element size	h_e	$h_e \lesssim \lambda_{\min}/N_\lambda$, with $N_\lambda \approx 6$–12	Controls FEM/BEM accuracy and computational cost
Nodes per wavelength	N_λ	Tuned to balance dispersion error and run time	Higher N_λ needed near strong gradients or scatterers
Time step (FDTD)	Δt	$\Delta t \le \Delta x/(c_0\sqrt{3})$ in 3D	Imposes stability limit for transient simulations at high resolution

Table 5 Meshing and timestep guidelines linking frequency content to numerical resolution requirements.

Because single-record periodograms are noisy, averaging methods are commonly used. A Welch-style estimator partitions the record into overlapping segments, applies a taper, computes periodograms, and averages them to reduce variance. In simulation, variance can also arise from stochastic excitation components representing tread pattern or lateral wander, so averaging across realizations can be used to obtain stable spectral signatures.

Time–frequency analysis is helpful for capturing the evolution from the initial impact into steady periodic excitation. The short-time Fourier transform (STFT) of $p(t)$ with window function $g(t)$ is [14]

$$\mathcal{P}(t,\omega) = \int_{-\infty}^{\infty} p(\tau) g(\tau - t) e^{-i\omega\tau}\, d\tau.$$

The spectrogram $|\mathcal{P}(t,\omega)|^2$ reveals whether energy is concentrated in stationary bands or appears as bursts aligned with strip encounters. In predictive modeling, features derived from the spectrogram such as band-integrated energy or modulation depth can improve mapping from geometry to perceived loudness, since human response can be sensitive to modulation and tonal prominence.

Environmental noise practice often employs frequency weighting and banding. A-weighted SPL, denoted $L_{p,A}$, applies a frequency-dependent weighting $W_A(f)$ that approximates human sensitivity at moderate levels. In spectral terms, if $S_{pp}(f)$ is the PSD, an A-weighted mean-square pressure can be computed as

$$p^2_{A,\mathrm{rms}} = \int_0^{\infty} W_A^2(f) S_{pp}(f)\, df,$$

and the corresponding level is $L_{p,A} = 10\log_{10}\left(p^2_{A,\mathrm{rms}}/p^2_{\mathrm{ref}}\right)$. Band-limited descriptors such as 1/3-octave band levels aggregate energy over logarithmically spaced bands. If a band spans frequencies $[f_1, f_2]$, the band mean-square pressure is

$$p^2_{\mathrm{band}} = \int_{f_1}^{f_2} S_{pp}(f)\, df,$$

and the band level is $L_{\mathrm{band}} = 10\log_{10}\left(p^2_{\mathrm{band}}/p^2_{\mathrm{ref}}\right)$. These band levels can reveal which harmonics dominate and how design changes shift energy across bands.

Propagation from the source region near the tire to external receivers is shaped by geometric spreading, reflection, atmospheric absorption, and scattering. In free space, a compact source yields a $1/R$ decay of pressure amplitude, implying a $20\log_{10}(R)$ decay in level. Near a ground plane, interference between direct and reflected paths produces frequency-dependent amplification or attenuation. For a rigid ground, the reflected wave has approximately the same magnitude as the direct wave with a phase shift determined by path-length difference. If R_d is the direct path length and R_r the reflected path length, a simplified pressure amplitude model is

$$p(\omega) \propto \frac{e^{-ikR_d}}{R_d} + \frac{e^{-ikR_r}}{R_r},$$

and the magnitude squared produces comb-filter-like ripples. Introducing ground impedance modifies the reflection coefficient to be complex and frequency dependent [15]. A common representation uses a plane-wave reflection coefficient $R(\omega,\theta)$ that depends on incidence angle θ and normalized impedance $Z(\omega)$:

$$R(\omega,\theta) = \frac{Z(\omega)\cos\theta - 1}{Z(\omega)\cos\theta + 1}.$$

While this plane-wave formula is limited for finite sources and near-field conditions, it provides insight into how softer ground can reduce destructive and constructive

Metric	Symbol	Definition (schematic)	Use in rumble-strip assessment
Sound pressure level	L_p	$20\log_{10}(p_{\mathrm{rms}}/p_{\mathrm{ref}})$	Baseline external noise indicator over selected windows
A-weighted SPL	$L_{p,A}$	From $W_A(f)S_{pp}(f)$ integrated over frequency	Aligns predictions with human loudness perception and regulations
Band level	L_{band}	$10\log_{10}(p^2_{\mathrm{band}}/p^2_{\mathrm{ref}})$	Reveals how designs redistribute energy across bands
Time–frequency energy	Spectrogram	$\lvert\mathcal{P}(t,\omega)\rvert^2$ via STFT	Separates entry/exit transients from steady harmonic components
Tonal prominence	ΔL_h	Log ratio of harmonic-band to background energy	Quantifies tonal character linked to strip spacing and speed
Event aggregation	Traversal / steady metrics	Different window placements for full pass vs central periodic segment	Distinguishes exposure measures from quasi-stationary behavior

Table 6 Noise and spectral descriptors derived from simulated pressure signals at roadside receivers.

extremes, often lowering mid-frequency peaks but potentially increasing some low-frequency components through phase changes.

Atmospheric absorption can be incorporated as an exponential decay with distance that increases with frequency. A pragmatic frequency-domain representation modifies the wavenumber to be complex, $k \to k + i\alpha(\omega)$, where $\alpha(\omega)$ is an attenuation coefficient. The pressure term e^{-ikR}/R becomes $e^{-ikR}e^{-\alpha(\omega)R}/R$, leading to frequency-dependent level reductions. Temperature and humidity influence $\alpha(\omega)$, and in predictive modeling these can be treated as covariates or uncertain parameters. For short roadside distances, absorption may be minor below 1–2 kHz but can become relevant at higher frequencies, particularly for receivers tens of meters away.

A key advantage of acoustic simulation is the ability to compute not only a single receiver level but a spatial map of sound pressure around the roadway. This supports analysis of how receiver height, setback distance, and barrier geometry affect predicted levels. For example, if $p(\mathbf{x},\omega)$ is computed on a grid of receiver locations, one can compute contours of $L_p(\mathbf{x})$ or $L_{p,A}(\mathbf{x})$ and identify regions where ground interference produces local maxima. Such maps also help diagnose whether a proposed design change reduces noise uniformly or merely redistributes it, which matters for multi-receptor optimization.

Because rumble-strip noise can exhibit strong harmonic structure, it is also helpful to define tonal metrics. One technical route is to compute a prominence ratio comparing energy in a narrow band around a harmonic to energy in adjacent bands [16]. If E_h is energy in a harmonic band and E_b is a background estimate, a log-based prominence measure can be defined as

$$\Delta L_h = 10\log_{10}\left(\frac{E_h}{E_b}\right).$$

In predictive modeling, ΔL_h can be used alongside overall levels to capture whether a design is likely to produce a distinct tonal character even when broadband level changes are modest. Since the perceptual and annoyance implications of tonality vary by context, reporting both overall and tonal descriptors supports neutral technical evaluation without presupposing a single outcome measure.

5. Predictive Statistical Modeling and Hypothesis Testing

A predictive model for external rumble-strip noise must reconcile two sources of complexity. First, the mapping from geometry and operating conditions to radiated noise is nonlinear and frequency dependent. Second, real-world variability from tires, vehicles, and environmental conditions can be large relative to design-induced changes. A statistically principled approach treats simulation outputs as structured information that constrains the functional form while allowing stochastic terms to capture variability and model discrepancy. The goal is not to replace physics with regression, but to use regression to compress physics into fast predictors and to quantify uncertainty and evidence for parameter effects.

Let $\mathbf{x} \in \mathbb{R}^d$ denote an input vector containing geometric and operational variables, for example strip spacing s, groove depth d_g, groove width w_g, edge radius r_e, pattern length L_p, vehicle speed V, lateral offset δ, and ground impedance parameters. Let y denote a noise metric such

Model family	Role in the framework	Advantages for external rumble-strip noise prediction
Linear / generalized linear regression	Baseline mapping from engineered features to metrics	Transparent coefficients, easy hypothesis testing, good for low-order sensitivities
Penalized regression (ridge, lasso, elastic net)	Handles enlarged feature sets and interactions	Controls overfitting, performs feature selection, supports interpretable sparsity
Gaussian process regression	Emulator for expensive simulations	Provides predictive distributions and length-scale-based sensitivity information
Tree-based ensembles (RF, boosting)	Flexible nonlinear predictors	Capture interactions and thresholds; useful mean models with post-hoc uncertainty tools
Multivariate / latent-factor models	Joint prediction of band levels or spectra	Exploit cross-frequency correlation and reduce dimensionality of response
Multi-fidelity co-kriging	Fusion of low- and high-fidelity simulations	Reduces high-fidelity runs while maintaining accuracy in sensitive regions of design space

Table 7 Representative statistical learning components used to emulate and interpret noise predictions.

as $L_{p,A}$ at a specified receiver location, or a vector of band levels. A baseline regression model is

$$y = f(\mathbf{x}) + \varepsilon,$$

where f is an unknown function and ε is a residual capturing unmodeled variability [17]. In many settings, a partially linear structure improves interpretability by separating known transformations from flexible components. For example, because SPL involves a logarithm, it can be useful to model mean-square pressure on a linear scale and then transform. If u denotes predicted mean-square pressure, one can model

$$\log u = g(\mathbf{x}) + \eta,$$

and then compute $L_p = 10 \log_{10}(u/p_{\text{ref}}^2)$. This ensures positivity of u and can stabilize variance.

Descriptive statistics provide an initial characterization of simulation ensembles or measured datasets used for calibration. For each metric y, the sample mean $\bar{y}$, variance s_y^2, skewness, and quantiles indicate whether the distribution is approximately symmetric or heavy-tailed. If repeated runs differ due to stochastic excitation components, one can estimate within-condition variance and compare it to between-condition variance induced by geometry changes. A useful ratio is

$$\text{SNR}_{\text{geom}} = \frac{\text{Var}(\mathbb{E}[y|\mathbf{x}])}{\mathbb{E}[\text{Var}(y|\mathbf{x})]},$$

which, when greater than 1, indicates that geometry-driven effects are at least comparable to stochastic variability. If this ratio is low, predictive intervals will be wide and optimization should be cautious about over-interpreting small differences.

For parametric interpretability, generalized linear models or polynomial regressions can be used as a first layer [18]. Suppose $f(\mathbf{x})$ is approximated as $f(\mathbf{x}) = \mathbf{z}(\mathbf{x})^\top \boldsymbol{\beta}$ where $\mathbf{z}(\mathbf{x})$ is a feature vector including nonlinear transforms such as V/s for encounter rate, $k_s L_c$ for patch-resolution, and interactions like $(d_g)(V/s)$. Then $\boldsymbol{\beta}$ can be estimated by least squares or penalized methods. With n observations, the ridge estimator solves

$$\hat{\boldsymbol{\beta}} = \arg\min_{\boldsymbol{\beta}} \|\mathbf{y} - \mathbf{Z}\boldsymbol{\beta}\|_2^2 + \lambda \|\boldsymbol{\beta}\|_2^2,$$

while the lasso replaces the ℓ_2 penalty with ℓ_1. Elastic net combines both. Penalization is useful because feature sets can be large when including frequency-band descriptors and interactions. Coefficient magnitudes then provide a rough sense of sensitivity, but interpretation should account for feature scaling.

Hypothesis testing can be used to assess whether certain geometric parameters have statistically discernible effects given noise and sample size. In a linear regression with Gaussian errors, a test of $H_0 : \beta_j = 0$ uses a t statistic

$$t_j = \frac{\hat{\beta}_j}{\text{SE}(\hat{\beta}_j)},$$

where SE is the standard error. If residual variance is heteroscedastic, robust standard errors can be used. When comparing nested models, an F test or likelihood-ratio test can assess whether adding a set of features improves fit beyond chance. In the present application, hypothesis tests should be interpreted as evidence within the

Aspect	Diagnostic	Interpretation for model credibility
Overall level accuracy	Errors in L_p or $L_{p,A}$ across conditions	Checks global bias in predicted external levels vs measurements
Band-level structure	Residuals in L_{band} or spectra	Reveals missed harmonic content or mis-modeled high-frequency roll-off
Predictive uncertainty	Standardized residuals r_i	Assesses calibration of uncertainty; large tails indicate underestimation of variability
Speed and spacing trends	Error vs V, s, or V/s	Identifies deficiencies in excitation scaling and propagation at different encounter rates
Within-condition variability	Measured vs modeled variance across passes	Tests stochastic source representations (tread pattern, wander, fleet mix)
Cross-validation layout	Hold-out by geometry / speed blocks	Evaluates extrapolation reliability to new designs rather than repeated conditions

Table 8 Validation and uncertainty checks linking predictions to field or experimental measurements.

modeling assumptions rather than as definitive causal claims, particularly because simulation-based datasets may not reflect all real-world confounders. Nevertheless, tests can identify which parameters are consistently influential across conditions and which appear negligible relative to uncertainty [19].

Because the response surface may be highly nonlinear, nonparametric or semi-parametric models are often appropriate. Gaussian process regression provides a probabilistic emulator with a kernel that encodes smoothness assumptions. If $f(\mathbf{x})$ is modeled as a Gaussian process with mean $m(\mathbf{x})$ and covariance $K(\mathbf{x}, \mathbf{x}')$, then for observed data $\mathbf{y}$ at inputs $\{\mathbf{x}_i\}$, the predictive distribution at a new input $\mathbf{x}_*$ is Gaussian with mean and variance derived from kernel matrices. A squared-exponential kernel,

$$K(\mathbf{x}, \mathbf{x}') = \sigma_f^2 \exp\left(-\frac{1}{2}\sum_{j=1}^{d}\frac{(x_j - x_j')^2}{\ell_j^2}\right),$$

implies smooth dependence with characteristic length scales ℓ_j. These length scales can indicate which variables the response changes rapidly with, providing a sensitivity interpretation. If the response includes periodic dependence on V/s, kernels with periodic components can capture harmonic structure without requiring explicit feature engineering.

Alternative learners such as random forests or gradient-boosted trees can model nonlinear interactions and discontinuities. However, their predictive uncertainty is less straightforward unless specialized methods are used. A useful compromise is to use such models as mean predictors and to estimate uncertainty via quantile regression, conformal prediction, or Bayesian additive regression trees. For engineering decisions, uncertainty intervals are often more informative than marginal improvements in point accuracy because they indicate whether differences between designs exceed variability [20].

An important aspect of predictive modeling in this context is multi-output structure. One may predict a vector $\mathbf{y}$ of B band levels or spectral features rather than a single scalar. Modeling each band independently ignores cross-frequency correlation induced by shared excitation and propagation. A multivariate Gaussian process or a latent-factor model can capture shared structure. For example, one can represent band levels as

$$\mathbf{y}(\mathbf{x}) = \mathbf{A}\mathbf{h}(\mathbf{x}) + \boldsymbol{\varepsilon},$$

where $\mathbf{h}(\mathbf{x})$ is a lower-dimensional latent vector modeled by Gaussian processes and $\mathbf{A}$ is a loading matrix. This reduces the dimensionality of the learning problem and preserves coherent spectral shifts with geometry changes. It also facilitates reconstruction of overall A-weighted levels from predicted spectra.

Calibration against measurements can be formulated as an inference problem where uncertain simulation parameters are estimated to match observed data. Let $\boldsymbol{\phi}$ denote uncertain parameters such as effective tire stiffness, modal damping, ground impedance scalars, or source directivity coefficients. The simulation predicts $y_{\text{sim}}(\mathbf{x}, \boldsymbol{\phi})$,

Category	Example expression	Purpose in design and decision-making
External noise objective	Minimize $Q_q(\mathbf{x})$ for q-quantile of $L_{p,A}$	Target robust reduction of high-end external levels at key receivers
Robustness to uncertainty	Include $\mu(\mathbf{x}) + \kappa\sigma(\mathbf{x})$ in cost	Penalize designs that rely on optimistic assumptions or poorly constrained physics
Alerting / safety constraint	$A(\mathbf{x}) \geq A_{\min}$ based on force or in-vehicle proxy	Maintain minimum tactile or audible cue strength for safety performance
Geometric and implementation constraints	Bounds on s, d_g, w_g, pattern length, constructability	Ensure designs remain compatible with construction practice and maintenance
Multi-criterion exploration	Tradeoff curves between noise metrics and alerting measures	Visualize and negotiate compromises between community impact and safety objectives

Table 9 Illustrative objectives and constraints for optimization of transverse rumble-strip geometries under uncertainty.

while observations y_{obs} satisfy

$$y_{\text{obs}} = y_{\text{sim}}(\mathbf{x}, \boldsymbol{\phi}) + \delta(\mathbf{x}) + \epsilon,$$

where $\delta(\mathbf{x})$ is a model-discrepancy term and ϵ measurement noise. Treating $\delta(\mathbf{x})$ as a stochastic process avoids forcing parameter estimates to absorb structural simulation errors. Bayesian inference can then yield posterior distributions for $\boldsymbol{\phi}$ and predictive distributions for new designs. Even outside a fully Bayesian approach, regularized calibration that penalizes parameter deviation from plausible ranges can improve generalization.

Model evaluation should emphasize out-of-sample performance. If data include multiple speeds and geometries, cross-validation should be structured to avoid leakage, for example by holding out entire geometries so that the test set represents genuine design extrapolation [21]. Error metrics can be defined on decibel scales, but because decibels are logarithmic, differences correspond to ratios in mean-square pressure. If y is in dB, the mean absolute error MAE provides an interpretable measure of typical deviation. For spectral outputs, a weighted error can emphasize bands that contribute most to A-weighting or that contain dominant harmonics. A spectral error metric can be defined as

$$E_{\text{spec}} = \sum_{b=1}^{B} w_b \, (y_b - \hat{y}_b)^2 ,$$

with weights w_b normalized to sum to 1. If w_b are proportional to A-weighting contributions, the metric aligns with perceived impact while still retaining spectral structure.

6. Standards-Based Field Alignment and Design-Driven Noise Mitigation Pathways

A persistent barrier to actionable rumble-strip noise mitigation is the mismatch between what is easy to vary in simulation and what is credibly comparable to agency measurement protocols. For transverse rumble strips, the most decision-relevant quantities are rarely raw acoustic pressures at an arbitrary virtual point; they are standardized external descriptors computed over representative pass-by events under continuous traffic flow, together with in-vehicle increments that proxy alerting efficacy. When simulation workflows are structured to output the same class of time-integrated external descriptors and in-cabin deltas used in practice, the resulting predictors become easier to interpret and calibrate, and geometric tradeoffs can be expressed in the same technical language used for complaints and design exceptions. This section therefore frames a standards-consistent linkage between simulation outputs and field-style descriptors, and then uses that linkage to motivate parameter regimes that tend to lower external emissions while preserving in-vehicle increases.

A direct way to reconcile simulation and measurement is to formalize the external descriptor as an event-integrated functional of the pressure time history at a roadside receiver [22]. Let $p(t)$ denote simulated acoustic pressure over a pass-by event of duration T, and let $W(f)$ denote a frequency-weighting operator applied either in the frequency domain or via an equivalent time-domain filter. The effective mean-square pressure can be written as $p_{\text{eff}}^2 = \frac{1}{T}\int_0^T \left(p_W(t)\right)^2 dt$, where $p_W(t)$ is the weighted pressure. The corresponding level is $L = 10\log_{10}\left(p_{\text{eff}}^2/p_{\text{ref}}^2\right)$. In simulation-based parametric sweeps, it is often tempting to compare unweighted peak values because they are visually salient, but peaks can be dominated by entry or exit transients that may not govern time-integrated descriptors under continuous-flow conditions. A more robust comparison is obtained by computing the same time-integrated or traversal-integrated functional for each geometry and speed, and then aggregating across a traffic distribution, for example by

defining an expected descriptor $\mathbb{E}[L|\boldsymbol{\theta}]$ under a speed probability density $p(V)$. This expectation can be approximated by quadrature or Monte Carlo sampling as $\mathbb{E}[L|\boldsymbol{\theta}] \approx \frac{1}{M}\sum_{m=1}^{M} L(\boldsymbol{\theta}, V_m)$ with $V_m \sim p(V)$, ensuring that the predicted effect of spacing, which shifts harmonic content as $f_0 = V/s$, is averaged over realistic speed variability rather than tied to a single nominal value.

Within such a standards-aligned evaluation, the design variables that most consistently control exterior emissions are those that directly scale the magnitude and sharpness of the contact excitation. For a simplified excitation model, if the strip profile input is $u(t) = z_s(Vt; \boldsymbol{\theta})$ and the transmitted force spectrum is $F(\omega) = H_F(\omega)U(\omega)$ for some mechanical transfer function H_F, then geometric changes that reduce the amplitude of $U(\omega)$ in the band where $|H_F(\omega)|$ is large will reduce the radiated field. Shorter and shallower patterns can accomplish this in two ways that are distinguishable in the spectrum. First, reducing groove depth reduces the low-order harmonic magnitudes in $U(\omega)$ and lowers the overall force variance $\mathrm{Var}(F)$, which tends to reduce broadband radiation. Second, reducing the effective pattern length reduces the time over which steady periodic excitation persists, which can lower time-integrated descriptors even when instantaneous spectral peaks remain visible, because the integral $\int_0^T (p_W(t))^2 dt$ scales with both amplitude and duration. These mechanisms are compatible with field-oriented observations that geometries with reduced depth and reduced overall pattern extent can yield measurable decreases in external descriptors while retaining an in-vehicle perceptual cue, since in-cabin response is influenced not only by absolute acoustic power but also by vibrational transmission paths and cabin filtering that can preserve a relative increase even when exterior radiation is moderated.

An implicit but useful constraint arises when in-vehicle alerting is framed as a required increase relative to baseline pavement noise rather than an absolute target. Let $L_{\mathrm{cab,base}}$ be the in-cabin level on the approach pavement without the strips and $L_{\mathrm{cab,trs}}(\boldsymbol{\theta}, V)$ the in-cabin level while traversing the strip array. Define $\Delta L_{\mathrm{cab}}(\boldsymbol{\theta}, V) = L_{\mathrm{cab,trs}} - L_{\mathrm{cab,base}}$. If an alerting guideline is expressed as $\Delta L_{\mathrm{cab}} \in [\Delta_{\min}, \Delta_{\max}]$ with $\Delta_{\min} = 3$ dBA and $\Delta_{\max} = 15$ dBA, then the feasible design space is the set of $\boldsymbol{\theta}$ for which $\mathbb{P}(\Delta_{\min} \le \Delta L_{\mathrm{cab}}(\boldsymbol{\theta}, V) \le \Delta_{\max})$ is sufficiently high under expected speed distributions. Empirically grounded field work indicates that reducing depth and overall pattern extent can still satisfy such a constraint while decreasing external descriptors, implying that the in-cabin transfer from contact excitation to cabin SPL can remain adequately sensitive even when the exterior radiation path is partially suppressed (Sallam et. al (2025)). In a predictive modeling context, this motivates a bi-criteria mapping in which the external metric is minimized subject to a probabilistic in-cabin constraint, rather than assuming that any reduction in contact excitation necessarily undermines alerting.

When reported changes are expressed as percentage reductions in external descriptors across designs, a careful interpretation is required because decibel quantities are logarithmic. If a descriptor is defined on a linear mean-square scale p_{eff}^2, a fractional reduction by r implies $p_{\mathrm{eff,new}}^2 = (1-r)p_{\mathrm{eff,old}}^2$, and the corresponding decibel change is $\Delta L = 10\log_{10}(1-r)$. For $r = 0.03$, $\Delta L \approx 10\log_{10}(0.97)$, and for $r = 0.08$, $\Delta L \approx 10\log_{10}(0.92)$, both yielding modest negative shifts in dB because the log compresses linear changes. If instead the percentage refers to the decibel value itself, $L_{\mathrm{new}} = (1-r)L_{\mathrm{old}}$, then the implied absolute dB change depends on the baseline level, which can produce larger shifts for high baselines. Because field summaries often communicate reductions as percentages for readability, simulation-to-field alignment benefits from reporting both the absolute decibel differences and the implied linear ratios, so that design decisions are not inadvertently driven by ambiguous scaling. In the present framework, simulated outputs can be carried on a linear energy scale internally for aggregation, uncertainty propagation, and averaging across vehicles, and then mapped to decibels at the reporting stage, which yields consistent treatment of mixtures and avoids artifacts that can arise when averaging dB values directly.

A standards-consistent calibration loop can be expressed as a statistical mapping from geometry and operating conditions to external descriptors, with priors informed by mechanistic expectations. Let y_{ext} denote a time-integrated external descriptor and let y_{cab} denote the in-vehicle increment. A joint predictive model can be written as

$$y_{\mathrm{ext}} = f_{\mathrm{ext}}(\boldsymbol{\theta}, V, \mathbf{g}) + \varepsilon_{\mathrm{ext}},$$
$$y_{\mathrm{cab}} = f_{\mathrm{cab}}(\boldsymbol{\theta}, V, \mathbf{h}) + \varepsilon_{\mathrm{cab}},$$

where $\mathbf{g}$ and $\mathbf{h}$ include nuisance parameters such as ground impedance surrogates, tire stiffness surrogates, and cabin transfer scalars, and where $(\varepsilon_{\mathrm{ext}}, \varepsilon_{\mathrm{cab}})$ capture residual variability across vehicle passes. The functions f_{ext} and f_{cab} can be constructed to incorporate simulation-derived features, for example harmonic amplitudes at $f_n = nV/s$, time-integrated band energies, and transient-to-steady ratios. A neutral but practically useful implication of reported field patterns is that the sign of the partial derivatives $\partial y_{\mathrm{ext}}/\partial d_g$ and $\partial y_{\mathrm{ext}}/\partial L_p$ is often positive over common design ranges, while $\partial y_{\mathrm{cab}}/\partial d_g$ may be positive but not so steep as to prevent meeting $\Delta_{\min}$ at reduced depths (Sallam et. al (2025)). Embedding such monotonicity as soft constraints or as regularization terms can stabilize regression when data are sparse, without asserting universality across all pavements and vehicle classes.

These relationships also suggest a pragmatic optimization problem that reflects how mitigation is discussed in practice, namely reducing external nuisance while maintaining alerting. One formulation minimizes an expected external level while enforcing the in-cabin constraint in

probability:

$$\min_{\boldsymbol{\theta}\in\Theta} \ \mathbb{E}[y_{\text{ext}}(\boldsymbol{\theta}, V)] \quad \text{subject to} \quad \mathbb{P}(y_{\text{cab}}(\boldsymbol{\theta}, V) \geq \Delta_{\text{min}}) \geq 1-\alpha,$$

with a small α controlling risk tolerance. If the predictive model is Gaussian with mean $\mu_{\text{cab}}(\boldsymbol{\theta})$ and standard deviation $\sigma_{\text{cab}}(\boldsymbol{\theta})$ after integrating over speed, then the constraint becomes $\mu_{\text{cab}}(\boldsymbol{\theta}) - z_{1-\alpha}\sigma_{\text{cab}}(\boldsymbol{\theta}) \geq \Delta_{\text{min}}$, where $z_{1-\alpha}$ is a normal quantile. This expresses, in a mathematically explicit way, the intuitive position that a design should not only meet the alerting threshold on average but should do so reliably across expected variability. In parallel, external mitigation can be pursued by penalizing spectral features associated with neighborhood complaints, which often correlate with tonal prominence and modulation depth [23]. A spectral penalty can be defined as $\Psi(\boldsymbol{\theta}) = \int w(f) \max\{0, \Delta L_h(f;\boldsymbol{\theta}) - \tau\}^2 df$, where ΔL_h is a tonal prominence measure and τ is a tolerance. Minimizing $\mathbb{E}[y_{\text{ext}}] + \gamma\Psi$ with a weight γ then encourages designs that reduce both overall level and pronounced spectral features without presupposing that one descriptor fully captures subjective response.

The field-compatibility perspective shows that mitigation claims should be conditional on pavement type and measurement geometry. Asphalt surfaces, through their texture and compliance, can alter both baseline tire noise and the incremental effect of transverse grooves. In the predictive framework, this can be represented by including pavement parameters that shift the baseline spectrum and the mechanical transfer function, so that the same geometric change does not imply a uniform external benefit across pavements. Even with this caveat, the convergence of physics-based reasoning and reported field tendencies supports a design hypothesis that is straightforward to test in simulation and measurement: reducing groove depth and reducing the effective length of the transverse pattern can yield measurable decreases in external, time-integrated descriptors while maintaining an in-vehicle increment within a target range for a substantial portion of operating conditions [24]. In a neutral technical sense, this hypothesis provides a tractable mitigation direction because it can be expressed directly in terms of controllable geometric parameters and can be evaluated using the same descriptor computation pipeline used for standards-driven assessments, thereby linking predictive modeling outputs to the practical context in which complaints and design revisions are adjudicated.

7. Parametric Analysis, Optimization, and Validation Under Uncertainty

Design decisions regarding transverse rumble strips often require balancing multiple objectives and constraints. Safety considerations motivate sufficient vibration and in-vehicle audible cues, while community considerations motivate minimizing external noise at roadside receivers. A parametric analysis framework can quantify tradeoffs by exploring how external metrics respond to geometric and operational variables, while an optimization layer can propose candidate geometries that meet constraints. Because both simulation and statistical models are uncertain, the optimization should account for uncertainty to avoid selecting designs that appear favorable only under optimistic assumptions.

Let $\mathbf{x}$ denote controllable design parameters, primarily geometry, and let $\mathbf{c}$ denote context parameters such as speed distribution, fleet mix, and ground properties. Let $Y(\mathbf{x}, \mathbf{c})$ be a random variable representing an external noise metric due to variability in tires and conditions. A robust objective can be defined as minimizing an upper quantile, for example the q-quantile with $q = 0.9$, denoted $Q_q(\mathbf{x})$, subject to constraints on an alerting metric $A(\mathbf{x})$:

$$\min_{\mathbf{x}} \ Q_q(\mathbf{x}) \quad \text{subject to} \quad A(\mathbf{x}) \geq A_{\text{min}}.$$

If $A(\mathbf{x})$ is not directly modeled, a surrogate constraint can be used based on predicted contact-force variation or in-vehicle vibration proxies. The quantile objective can be approximated from predictive distributions produced by the statistical model, or from Monte Carlo sampling if a fast emulator is available.

Sensitivity analysis helps identify which parameters matter most and whether effects are monotonic or involve interactions [25]. A local sensitivity of the mean response $\mu(\mathbf{x}) = \mathbb{E}[Y|\mathbf{x}]$ can be quantified by gradients $\nabla_{\mathbf{x}}\mu$. If the predictive model is differentiable, gradients can be computed analytically; otherwise they can be estimated by finite differences:

$$\frac{\partial \mu}{\partial x_j} \approx \frac{\mu(\mathbf{x} + \Delta x_j \mathbf{e}_j) - \mu(\mathbf{x} - \Delta x_j \mathbf{e}_j)}{2\Delta x_j}.$$

Because decibel responses can be nonlinear in geometry, gradient magnitudes can vary strongly across the design space, so sensitivity maps rather than single numbers are more informative. Global sensitivity can be assessed through variance-based measures. If inputs are treated as random variables with a specified distribution, the total variance $\text{Var}(Y)$ can be decomposed into contributions from each input and from interactions. A Sobol-style first-order index for variable x_j is

$$S_j = \frac{\text{Var}\left(\mathbb{E}[Y|x_j]\right)}{\text{Var}(Y)},$$

with total-effect indices capturing interactions. When computed using an emulator, these indices can be obtained efficiently and can guide whether optimization should focus on a subset of parameters.

Optimization can be carried out using gradient-based methods when the response is smooth, or derivative-free methods when discontinuities arise, for example due to

contact-loss thresholds or resonance shifts. A typical unconstrained formulation on a penalty basis is

$$\min_{\mathbf{x}} \; J(\mathbf{x}) = \mu(\mathbf{x}) + \kappa\sigma(\mathbf{x}) + \rho \max\{0, A_{\min} - A(\mathbf{x})\}^2,$$

where $\sigma(\mathbf{x})$ is predictive standard deviation, κ controls risk aversion, and ρ is a penalty weight. The term $\mu + \kappa\sigma$ corresponds to minimizing an upper confidence bound, encouraging designs with both low mean and low uncertainty. This is particularly relevant when the available data sparsely cover the design space or when simulation discrepancy is significant [26]. In a Bayesian-optimization setting, $J(\mathbf{x})$ can serve as an acquisition function, selecting new simulation points that improve the emulator where it matters for design.

From a numerical perspective, an efficient optimization workflow leverages multi-fidelity modeling. Lower-fidelity simulations, such as simplified monopole or dipole source approximations with analytical ground reflection, can screen broad design ranges, while higher-fidelity FEM–BEM models refine promising candidates. The statistical model can integrate both fidelities using a co-kriging-like approach in which high-fidelity outputs are modeled as a correction to low-fidelity predictions:

$$y_H(\mathbf{x}) = \rho y_L(\mathbf{x}) + \Delta(\mathbf{x}),$$

where $\Delta(\mathbf{x})$ is a Gaussian process capturing discrepancy between fidelities. This approach can reduce total high-fidelity runs needed to achieve a target prediction accuracy. It also provides a structured way to combine mechanistic understanding at low cost with detailed acoustic scattering effects at higher cost.

Validation is central to establishing whether predictions are usable within expected tolerances. Validation should be framed as comparing predicted distributions to measured distributions rather than expecting perfect agreement at every frequency and position. For a set of measurement conditions indexed by i, with measured levels y_i^{meas} and predicted means $\hat{y}_i$ and predictive variances $\hat{\sigma}_i^2$, one can compute standardized residuals

$$r_i = \frac{y_i^{\text{meas}} - \hat{y}_i}{\hat{\sigma}_i},$$

and check whether the distribution of $\{r_i\}$ is approximately centered and has variance near 1. If residuals show systematic bias with speed, receiver height, or geometry, this indicates missing physics or mis-specified covariate dependence. Because rumble-strip noise can be sensitive to lateral position, validation should include controlled lateral offsets, or at least account for typical wander distributions. If measurements include multiple passes, within-condition variability can be compared with predicted variability to assess whether stochastic source components are appropriately represented.

Spectral validation is more diagnostic than overall-level validation because it reveals whether the model captures harmonic placement and bandwidth [27]. If L_b^{meas} and $\hat{L}_b$ are measured and predicted band levels, one can compute a bandwise error vector and examine whether errors cluster around harmonic bands. Systematic underprediction at harmonics could indicate insufficient representation of edge sharpness or contact-force impulsiveness, while overprediction at high frequencies could indicate overly rigid ground assumptions or insufficient atmospheric attenuation. Because the decibel scale compresses large energy differences, it can also be useful to validate on linear mean-square pressure in selected bands to ensure that energetic contributions are not being obscured.

Uncertainty quantification should include parametric uncertainty and model-form uncertainty. Parametric uncertainty arises from unknown values of tire stiffness, damping, and ground impedance, which can be represented as probability distributions. Model-form uncertainty arises from simplifying assumptions such as linear contact, reduced-order source radiation, or locally reacting ground. A practical way to represent model-form uncertainty is to include a discrepancy term with a correlation structure across frequencies and operating conditions. For example, for band levels y_b, one can model discrepancy as a multivariate normal with covariance

$$\operatorname{Cov}(\delta_b, \delta_{b'}) = \sigma_\delta^2 \exp\left(-\frac{|\log f_b - \log f_{b'}|}{\ell_f}\right),$$

which encodes that discrepancies are smoother across log-frequency than across linear frequency. Incorporating this term prevents overconfidence in spectral details that are sensitive to modeling approximations. In optimization, including discrepancy tends to favor designs whose predicted advantage is robust across plausible discrepancy realizations [28].

A recurring design question is how geometric changes influence not only overall level but also the spectral distribution. Increasing groove depth, for example, may increase low-frequency force variation and thus excite structural and cavity modes, while sharpening edges may increase high-frequency content through impulsive contact. Spacing changes primarily shift harmonic locations through $f_0 = V/s$, potentially moving energy into bands where ground interference is constructive or where A-weighting is higher. Parametric analysis can isolate these mechanisms by holding certain combinations constant, such as maintaining the same encounter rate while varying depth, or maintaining the same depth while shifting spacing. Such analyses can be formalized by exploring manifolds in parameter space defined by constraints, for instance $V/s = \text{const}$, and evaluating predicted outcomes along those manifolds.

While this framework focuses on airborne exterior noise, it is technically consistent to compute related quantities such as radiated sound power under controlled boundary conditions. If an enclosing surface S surrounds the source region and the acoustic intensity

is approximated as $I_n \approx \frac{1}{2}\mathrm{Re}\{p v_n^*\}$ under harmonic conditions, then radiated power is

$$W = \int_S I_n \, dS,$$

and sound power level is

$$L_W = 10 \log_{10}\left(\frac{W}{W_{\mathrm{ref}}}\right).$$

Sound power is less dependent on receiver placement than SPL and can therefore provide a more source-centric metric for comparing geometries. However, environmental impact depends on propagation, so both perspectives are useful. When integrating sound power into predictive models, care is needed because the mapping from power to receiver SPL depends on directivity and ground effects, which may vary with frequency and vehicle configuration.

8. Conclusion

This paper presented an integrated methodology for predicting external acoustic emissions generated by vehicles traversing transverse rumble strips, combining mechanistic source characterization, numerical acoustic simulation, and statistical learning [29]. The development framed the rumble-strip geometry as a parametric surface profile that induces a speed-dependent excitation signal at the tire–pavement contact. Reduced-order dynamical representations were used to translate profile-induced displacement into contact forces and into equivalent radiating boundary conditions, enabling coupling to linear acoustic propagation models. Frequency-domain formulations based on the Helmholtz equation and time-domain wave formulations were described as complementary tools, with FEM, BEM, and coupled FEM–BEM approaches providing pathways to capture near-field complexity and far-field radiation in an unbounded environment. Resolution constraints, radiation treatments, and ground-impedance effects were emphasized because they strongly influence predicted spectral structure and receiver levels.

Signal-processing components were articulated to convert simulated pressure time histories into decibel-based metrics and spectral descriptors, including band levels, weighted levels, and time–frequency representations that reflect the quasi-periodic and transient components of rumble-strip noise. Propagation modeling considerations such as ground interference and atmospheric absorption were incorporated as mechanisms that reshape emitted spectra at roadside receivers, often producing frequency-selective amplification that interacts with strip spacing and vehicle speed. The statistical modeling layer was formulated to map geometric and operational variables to predicted noise metrics while quantifying uncertainty, supporting hypothesis tests for parameter effects, and enabling multi-output spectral prediction. Emulation, calibration, and cross-validated evaluation were described as practical elements for building predictors that remain useful when direct high-fidelity simulation at every design point is infeasible.

Finally, the framework was extended to parametric analysis and optimization under uncertainty, highlighting how robust objectives and uncertainty-aware constraints can guide design modifications that reduce external noise without presuming that a single deterministic prediction is sufficient. The overall result is a technical workflow that can support comparative assessment of rumble-strip geometries, exploration of tradeoffs between spectral characteristics and overall levels, and structured incorporation of limited field data for calibration and validation. The approach does not eliminate the need for measurements, but it provides a systematic way to generalize beyond measured configurations and to make design decisions with explicit recognition of variability and model limitations [30].

References

[1] A. Crawford, A. Kiley, K. A. Loparo, M. L. Audu, and R. J. Triolo, "Detecting destabilizing wheelchair conditions for maintaining seated posture.," *Disability and rehabilitation. Assistive technology*, vol. 13, pp. 178–185, 4 2017.

[2] J. A. Adedeji, X. E. Feikie, T. C. Dzogbewu, and M. M. H. Mostafa, "Reaction behaviour of drivers to marked and unmarked road: Ghana perspective," *Put i saobraćaj*, vol. 67, pp. 1–6, 3 2021.

[3] M. Ramaraj, D. Sabareeswaran, V. Vijayalaksmi, C. Jothish, N. Thangarasu, and G. Manivasagam, "Sophisticated cpbis methods applied for fbisodata clustering algorithm using with real time image database," *Indonesian Journal of Electrical Engineering and Computer Science*, vol. 30, pp. 614–614, 4 2023.

[4] A. C. Lusk, W. C. Willett, V. Morris, C. Byner, and Y. Li, "Bicycle facilities safest from crime and crashes: Perceptions of residents familiar with higher crime/lower income neighborhoods in boston," *International journal of environmental research and public health*, vol. 16, pp. 484–, 2 2019.

[5] R. Shah and M. Alqarni, "An investigation of health and safety issues at highway construction sites in developing countries," *Journal of Advanced College of Engineering and Management*, vol. 4, pp. 83–93, 12 2018.

[6] Q. Hussain, W. K. Alhajyaseen, N. Reinolsmann, K. Brijs, A. Pirdavani, G. Wets, and T. Brijs, "Optical pavement treatments and their impact on speed and lateral position at transition zones: A driving simulator study.," *Accident; analysis and prevention*, vol. 150, pp. 105916–, 12 2020.

[7] C. Heine and S. Feldman, "Technology and older women: Considerations regarding their use and misuse.," *Frontiers in public health*, vol. 10, pp. 853983–, 6 2022.

[8] R. Armitage and L. Monchuk, "What is cpted? reconnecting theory with application in the words of users and abusers," *Policing: A Journal of Policy and Practice*, vol. 13, pp. 312–330, 3 2017.

[9] S. Cafiso and G. Pappalardo, "Safety effectiveness and performance of lane support systems for driving assistance and automation - experimental test and logistic regression for rare events.," *Accident; analysis and prevention*, vol. 148, pp. 105791–105791, 10 2020.

[10] D. Braslau and E. Terhaar, "Rumble strip sound level evaluation—comparison of three designs," *Journal of the Acoustical Society of America*, vol. 137, pp. 2319–2319, 4 2015.

[11] Y. Ma, W. Zhang, X. Gu, and J. Zhao, "Impacts of experimental advisory exit speed sign on traffic speeds for freeway exit ramp," *PloS one*, vol. 14, pp. 1–17, 11 2019.

[12] D. R. Large, G. Burnett, V. Antrobus, and L. Skrypchuk, "Driven to discussion: engaging drivers in conversation with a digital assistant as a countermeasure to passive task-related fatigue," *IET Intelligent Transport Systems*, vol. 12, pp. 420–426, 3 2018.

[13] F. Rosey, J.-M. Auberlet, J. Bertrand, and P. Plainchault, "Impact of perceptual treatments on lateral control during driving on crest vertical curves: A driving simulator study," *Accident; analysis and prevention*, vol. 40, pp. 1513–1523, 4 2008.

[14] C.-K. Toh, J. A. Sanguesa, J. C. Cano, and F. J. Martinez, "Advances in smart roads for future smart cities.," *Proceedings. Mathematical, physical, and engineering sciences*, vol. 476, pp. 20190439–20190439, 1 2020.

[15] A. Buczaj, A. Pecyna, M. Krzywicka, and A. Maruszewska, "Phenomenon of fatigue among professional drivers in poland.," *Annals of agricultural and environmental medicine : AAEM*, vol. 28, pp. 114–121, 5 2020.

[16] "Green highways-a sustainable approach," *International Journal of Environment and Health Sciences*, vol. 2, 8 2021.

[17] S. R. Passmore, N. Mortaza, C. M. Glazebrook, B. Murphy, and T. D. Lee, "Somatosensory integration and masking of complex tactile information: Peripheral and cortical contributions.," *Brain sciences*, vol. 10, pp. 954–, 12 2020.

[18] K. L. S. Bernhardt, M. R. Virkler, and N. M. Shaik, "Evaluation of supplementary traffic control measures for freeway work-zone approaches," *Transportation Research Record: Journal of the Transportation Research Board*, vol. 1745, pp. 10–19, 1 2001.

[19] D. Braslau, E. Terhaar, and K. Fleming, "Centerline rumble strip sound level evaluation—comparison of four designs," *Journal of the Acoustical Society of America*, vol. 140, pp. 3094–3094, 10 2016.

[20] P. Watson, A. Whale, S. A. Mears, L. A. Reyner, and R. J. Maughan, "Mild hypohydration increases the frequency of driver errors during a prolonged, monotonous driving task," *Physiology & behavior*, vol. 147, pp. 313–318, 4 2015.

[21] M. Abdel-Aty and A. Pande, "Crash data analysis: Collective vs. individual crash level approach," *Journal of safety research*, vol. 38, pp. 581–587, 10 2007.

[22] R. Goel, P. Jain, and G. Tiwari, "Correlates of fatality risk of vulnerable road users in delhi.," *Accident; analysis and prevention*, vol. 111, pp. 86–93, 11 2017.

[23] S. F. Quan, L. K. Barger, M. D. Weaver, and C. A. Czeisler, "Saving lives or saving dollars: The trump administration rescinds plans to require sleep apnea testing in commercial transportation operators," *Southwest Journal of Pulmonary and Critical Care*, vol. 15, pp. 84–86, 8 2017.

[24] O. Sallam, K. El-Rayes, E.-J. Ignacio, R. Hajj, and M. Al-Ghzawi, "Mitigating external noise of transverse rumble strips and complaints from nearby neighborhoods," *Transportation Research Part D: Transport and Environment*, vol. 149, p. 105021, 2025.

[25] D. Ghosh, S. Jamson, P. D. Baxter, and M. W. Elliott, "Factors that affect simulated driving in patients with obstructive sleep apnoea.," *ERJ open research*, vol. 1, pp. 00074–2015, 12 2015.

[26] T. Titchkosky, "The educated sensorium and the inclusion of disabled people as excludable," *Scandinavian Journal of Disability Research*, vol. 21, pp. 282–290, 12 2019.

[27] V. J. Gawron and T. A. Ranney, "The effects of rumble strips on performance of sober and alcohol-dosed subject drivers:," *Proceedings of the Human Factors Society Annual Meeting*, vol. 32, pp. 963–966, 10 1988.

[28] J. C. Choi, J. B. Lim, J. yeon Hong, and S. Y. Lee, "Study on the ways to improve deep underground road facilities and operation based on the cases of longitudinal tunnel," *Journal of the Korean Society of Safety*, vol. 30, pp. 122–131, 12 2015.

[29] J. Gooch, V. V. Gayah, and E. T. Donnell, "Quantifying the safety effects of horizontal curves on two-way,

two-lane rural roads," *Accident; analysis and prevention*, vol. 92, pp. 71–81, 4 2016.

[30] F. Westerhuis, A. B. M. Fuermaier, K. Brookhuis, and D. de Waard, "Cycling on the edge: the effects of edge lines, slanted kerbstones, shoulder, and edge strips on cycling behaviour of cyclists older than 50 years," *Ergonomics*, vol. 63, pp. 769–786, 4 2020.